Electrophoretic Separation of Long Polyelectrolytes in Submolecular-Size Constrictions: A Monte Carlo Study

Frédéric Tessier, Josée Labrie, and Gary W. Slater*

Department of Physics, University of Ottawa, 150 Louis-Pasteur, Ottawa, Ontario, Canada K1N 6N5

Received June 18, 2001; Revised Manuscript Received March 8, 2002

ABSTRACT: We use a bond-fluctuation Monte Carlo method to study the motion of long polyelectrolytes inside an array of microscopic entropic traps. The molecules are pulled through the array by an electric field and forced into submolecular-size constrictions between the larger trap regions. We numerically solve the Laplace equation inside the structure to obtain realistic field lines for our simulations. We find that the mobility of the molecules *increases* with molecular size and that the size-separation mechanism relies mainly on the overall deformation of the molecules as they approach the narrow constrictions. We also investigate specific aspects of the separation mechanism, namely the conformational behavior of the molecule, the hernia nucleation process, and the trapping time statistics as a function of molecular size and field strength. Our simulation results for the mobility, the critical hernia nucleation size, the mean trapping time, and the resolution are consistent with the experimental data and model previously published by Han et al.[1,2] Finally, we predict that such microfluidic structures could be used to separate topoisomers bearing the same molecular size.

I. Introduction

Microscopic devices that can detect, sort, purify, or otherwise manipulate individual particles, molecules, or even cells are bound to revolutionize molecular sciences, offering an unprecedented level of control in experimental settings. Molecular biology, in particular, will greatly benefit from such devices, not only because of the widespread interest in the analysis of biomolecules but also because large biomolecules are conveniently commensurate in size to the resolution of current microfabrication technologies. The growing thrust behind genomics is also pressing the need for more efficient ways to separate DNA fragments by size (a task pertinent to both gene mapping and sequencing); hence, many groups are currently working on the confection of micromachined separation systems that can outperform traditional gel electrophoresis methods. Proposed devices include sieves in the form of microscopic arrays of posts that mimic gel fibers,[3−5] Brownian rectifiers in the form of ratchets or asymmetric arrays of obstacles,[6−12] single-molecule sizing devices,[13] and entropic trapping systems.[1,2,14]

In this article we focus our attention on a microscopic entropic trap array recently fabricated by Han et al. and used for the separation of double-stranded DNA (dsDNA) fragments in the tens of kilobase pairs (kbp) range.[1,2] This array consists of a small channel with periodic constrictions etched on a silicon wafer, as depicted in Figure 1. The channel is about 1 μm across, and dsDNA molecules of a comparable size are pulled through the structure by a "low-intensity" electric field. The narrow constrictions, less than 0.1 μm across, hinder this motion, and longer molecules are found to advance *faster* overall than shorter ones. Questions pertaining to the origin and optimization of this rather counterintuitive size selectivity prompted us to investigate, through Monte Carlo simulations, the separation mechanisms at play in this device, where entropic forces prevail. Our results will show that longer molecules indeed have a higher mobility than shorter ones and that the separation process relies mostly on the overall size and deformation of the molecules as they travel through the channel. Furthermore, simulations enable us to investigate molecular behavior on the local scale, which can then be compared with theory. Overall, our conclusions agree with experimental data and the simple theoretical model proposed by Han et al.[1]

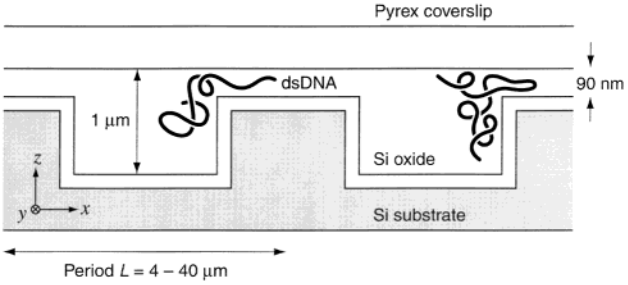

Figure 1. Schematic transverse cut of the microchannel device we are studying in this article (adapted from Han et al.[1]). Here the driving electric field is oriented toward the left so the (negatively charged) DNA strands migrate toward the right.

Before we present the outcome of our simulations, we briefly review our computational approach and some theoretical considerations. At the outset we should stress that the goal of this work is to characterize the generic mode of operation of the device and not to fit specific experimental data. We thus attempt to model the system in some level of detail to ensure that we operate in the appropriate regime and that we can establish a reliable qualitative correspondence with experiments, but we are not concerned with quantitative discrepancies that do not affect the nature of the separation process. Given its simple geometry, the structure studied in this article stands as a model pore-constriction system; hence, our results are also relevant in other contexts where macromolecules (i.e., flexible molecules with large internal conformational entropy)

* Corresponding author: e-mail gslater@science.uottawa.ca.

10.1021/ma0110406 CCC: $22.00
Published on Web 05/03/2002

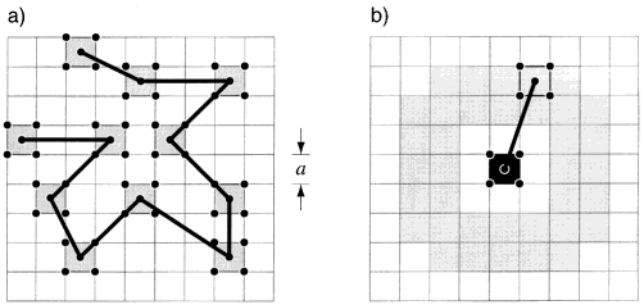

Figure 2. Bond fluctuation algorithm in two dimensions: (a) a sample walk on the bond fluctuation lattice, where each monomer occupies four lattice sites, and (b) the 36 allowed bond vectors between two successive monomers, the first of which is represented by the black square at the origin and the second one by a shaded square. This algorithm can be generalized in 3D, in which case each monomer occupies 8 lattice sites and there are 108 allowed bond vectors.

are forced through narrow slits or between large pores in a chemical gel.

II. Method

A. The Molecule and Its Dynamics. All the simulations reported in this article are based on the bond-fluctuation (BF) algorithm. This algorithm has been described in detail[15,16] and has been used extensively in polymer simulations, so we only recall its main characteristics. The simulation space is divided in unit cells so as to form an orthogonal lattice, and the macromolecule is represented by a chain of N effective monomers, each occupying 2^d lattice sites (where d is the dimensionality of space) to cover one unit cell (Figure 2a). A given lattice site can only belong to one monomer at a time in order to account for excluded volume interactions, and the bond vector connecting two successive monomers is constrained to a predefined set, chosen so as to avoid bond crossing; there are respectively 36 and 108 allowed bond vectors in 2D (Figure 2b) and 3D. In our case, each monomer also carries an effective electric charge q since we model a polyelectrolyte.

The motion of the chain is generated from local elementary moves: for each trial move, we randomly select a monomer and attempt to move it randomly by one lattice unit (which we denote by $a = 1$) along one of the axis directions. Provided that volume exclusion and bond constraints are respected, the move is accepted upon success of a Metropolis test[17] for the change in the electrostatic energy of the monomer (see below). The elementary time unit of the simulation is given by one Monte Carlo step (mcs), defined as N trial moves.

B. The Microchannel Device. The structure of the device sketched in Figure 1 is incorporated in the simulation by means of occupied lattice sites forming walls that match the device geometry. We use the lattice shown in Figure 3, with periodic boundary conditions (PBC) along the x and y directions. For conciseness, we refer to the large regions of the channel as *wells* and the constriction regions as *gaps*. We consider molecules with a radius of gyration (R_g) that is larger than half the gap size (so that there is trapping) yet smaller than half the well size (so that the molecule is not deformed between traps). If we assume that the average bond length in the simulations (roughly $2.8a$) is comparable to the persistence length of dsDNA (50 nm, or about 0.150 kbp), then we have $a \approx 20$ nm, hence our channel

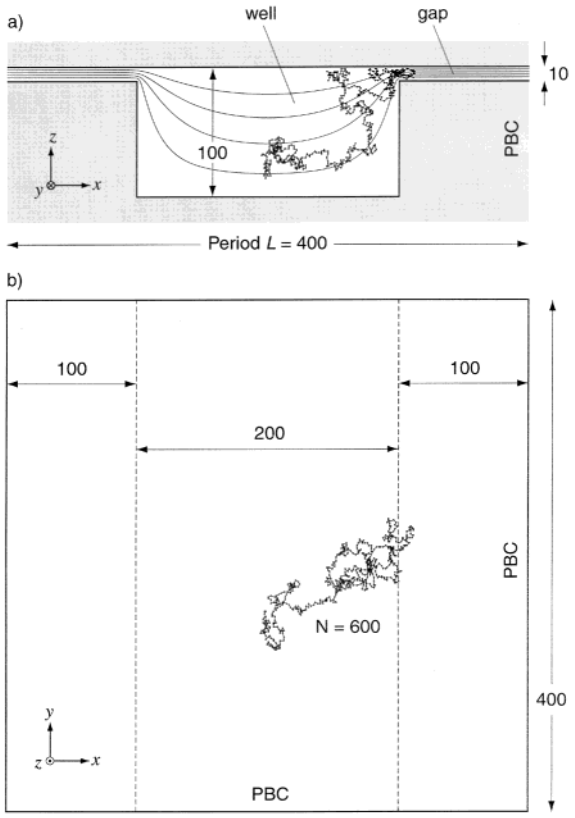

Figure 3. (a) A transverse (or xz) view of the lattice used for the 3D simulation of the microchannel device and (b) a top (or xy) view of the same system. The electric field lines are shown in the transverse view, and a sample molecule with $N = 600$ monomers is included. The dimensions of the lattice are all given in units of the lattice spacing ($a = 1$).

measures 2 μm across with a gap size of 200 nm, and it has a period L of 8 μm. The simulated chains vary in size from $N = 50$ to $N = 600$ effective monomers, which corresponds to dsDNA molecules ranging from 7 to 90 kbp. These numbers are all quite comparable to the dimensions reported by Han et al.[1]

We apply a potential difference ΔV_0 across the period L of our channel to model the driving electric field. The walls of the channel are considered perfect insulators, and we solve the Laplace equation numerically to obtain the local potential V on every lattice site. (We actually solve for the potential on a refined grid, and we take V as the average over the lattice cell of volume a^3 surrounding each site.) The resulting field lines are sketched in Figure 3a, and we verify that the electric field is stronger in the gap than in the well by a factor close to the ratio of the well size to the gap size, as it should. The Metropolis weight associated with the move of a monomer bearing a charge q is then simply given by $\exp(-q\delta V/k_BT)$, where δV is the potential difference between the two adjacent lattice sites involved, k_B is Boltzmann's constant, and T is the absolute temperature. The calculated potential drop across the periodic boundary in x is adjusted by ΔV_0 to obtain seamless field lines between successive sections of the periodic channel. Throughout this article, the strength of the applied field is always given in terms of the global dimensionless variable $\epsilon = q\Delta V_0 a/Lk_BT$. The field strength at the geometrical center of the gap is thus $\epsilon_{gap} \approx 1.8\epsilon$, whereas at the center of the well it is $\epsilon_{well} \approx 0.2\epsilon$.

C. Some Physical Elements That Are Omitted. We do not include solvent molecules in our simulations,

so explicit hydrodynamic interactions are neglected. Nevertheless, the free-draining electrophoretic property of polyelectrolytes is conveniently preserved in the Monte Carlo approach. However, the physical origin of this free-draining property is absent from our model, as it lies in the friction exerted locally on the chain by surrounding counterions. It is also important to keep in mind that the entropic forces that slow down (or trap) the DNA molecules at the well−gap interface are effectively mechanical forces that affect the free-draining properties of the polyelectrolyte, as discussed by Long et al. in a recent series of key articles.[18−21] These subtle effects are clearly not part of our model. (In fact, we are not aware of any Monte Carlo computer simulation study that currently addresses this issue.) One known effect is to reduce the magnitude of the mechanical force required to pin a polyelectrolyte in an electric field.[18,19] In our case, this implies that we underestimate by a factor $\approx L/R_g \sim N^{2/5}$ the field intensity needed to overcome the entropic potential barrier. However, we do not expect the basic trapping and detrapping mechanisms to be qualitatively affected by this discrepancy.

We do not consider the electroosmotic flow (EOF), and there is no otherwise imparted flow field inside the device; experimentally, the EOF is apparently quenched by the use of a high ionic strength buffer.[1] We obviously ignore intermolecular interactions as we simulate only one chain at a time, but modest polyelectrolyte concentrations are reported to only slightly affect the mobility and the separation capability of the device.[2] Apart from strict volume exclusion, we disregard interactions between the molecules and the walls of the channel, which are assumed perfectly flat and otherwise neutral. We neglect the bending energy of the macromolecule (however, our monomers already replace roughly one dsDNA persistence length) as well as the electrostatic repulsion between the charged monomers, although both of these aspects could play a role during trapping, when parts of the chain are typically highly bent and quite compact. Finally, we should mention that the bond-fluctuation algorithm implies rather bulky "monomers"; indeed, one effective monomer measures about 20 nm on a side (and, as mentioned previously, represents or replaces ≈150 bp), whereas the width of dsDNA for example is 10 times smaller. The algorithm can thus lead to spurious finite-size effects, especially in the limit of narrow passages such as in the channel gap. This is why we did not attempt to study even stronger confinement using this algorithm. The gap confinement studied here is fully consistent with that investigated experimentally.[1,2]

III. Theory

The mobility of the polyelectrolytes inside the channel is the physical quantity that can be best compared with available experimental data.[1,2] We recall that the electrophoretic mobility μ is defined through

$$v = \mu E \tag{1}$$

where v is the mean velocity of the molecule and $E = \Delta V_0/L$ is the global magnitude of the applied electric field. In a separation device, the mobility is typically a function of both field strength (E) and molecular size (N). In the simulations we obtain μ from v/ϵ and throughout this article we always present the mobility in terms of the dimensionless ratio μ/μ_0, where μ_0 is the mobility of a chain in free solution (no constraint). Note that μ_0 is practically independent of chain length and field strength for free-draining polyelectrolytes; hence, we regard it as a constant.

To explain the observed mobility of DNA in their microdevice, Han et al. have constructed a simple kinetic model,[1] which we briefly review here. They suggest that DNA escapes from the entropic trap by way of small hernias entering the high-field region inside the gap. (Such hernias are seen in Figure 3a,b, for example.) The escape of the whole chain is iniated once a hernia venturing inside the gap reaches a critical distance x_c, at which point the hernia simply pulls the chain through; i.e., it helps the chain overcome the entropic barrier. When a length x of DNA enters the gap longitudinally, the decrease in electrical potential energy is proportional to x^2E, while the increase in entropic free energy is proportional to xT (since conformational entropy is an extensive molecular property). The net free energy change caused by the hernia is thus $\Delta F \sim xT - x^2E$. This function reaches a maximum $\Delta F_{max} \sim T^2/E$, which represents the activation barrier for the escape of the molecule from the trap. This maximum occurs at a critical insertion length

$$x_c \sim T/E \sim 1/\epsilon \tag{2}$$

which can also be regarded as the critical hernia nucleation size (since a hernia reaching that size basically keeps growing). For moderate field intensities, the mean trapping time τ_{trap} can then be written in terms of the corresponding Boltzmann weight as

$$\tau_{trap} = \tau_0 \exp(\Delta F_{max}/k_BT) = \tau_0 \exp(\epsilon_0/\epsilon) \tag{3}$$

where ϵ_0 is independent of field strength and molecular size. The prefactor τ_0 on the other hand may depend on both E and N. According to eq 3, the molecules cannot escape from the trap without the help of an applied field, as the trapping time becomes infinite when the magnitude of the driving electric field vanishes. This is not completely realistic since the molecule could eventually diffuse out of the trap, but it is certainly reasonable over the time scale of our simulations.

Sebastian and Paul have developed a more detailed theory to treat the problem of a long macromolecule crossing a free energy barrier in one dimension.[22] The outcome of their calculations is consistent with the analysis above, and from their results we deduce that τ_0 should be proportional to $1/(N\sqrt{E})$ when escape occurs via hernia nucleation. If the molecule enters the gap head or tail first, then τ_0 should be independent of N, but this process is rare when N becomes large. Note, however, that the model they use implies that all monomers along the chain can simultaneously participate in the nucleation of hernias; hence, that the rate of escape is proportional to N.

The model reviewed here assumes that the hernias enter the gap longitudinaly, i.e., completely extended along the field direction. This may not be realistic when the field is weak since the entropic elasticity of the inserted hernia may exceed the electric forces acting on it, in which case it would retain a random coil conformation. We can easily generalize the model to take this aspect into account. For a contour length s inserted inside the gap, the entropic contribution remains proportional to sT, but the potential energy contribution now becomes proportional to $s^{1+\nu}E$ for a chain that extends over a distance s^ν inside the gap. (We can take

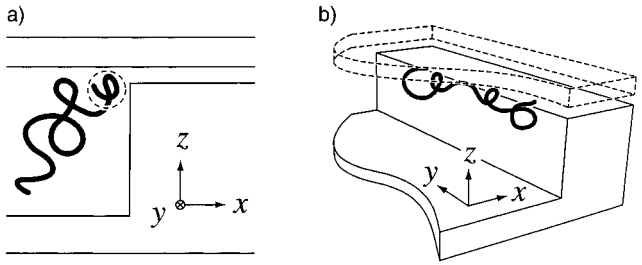

Figure 4. (a) If the molecule does not have the time to deform, only the monomers in the entrance blob close to the gap (represented by dashed circle) determine the escape dynamics; thus, increasing the chain length does not affect the escape process. (b) In this 3D view, we see how the molecule may deform and align itself along the gap axis; many escape blobs can then participate concurrently in the escape of the molecule.

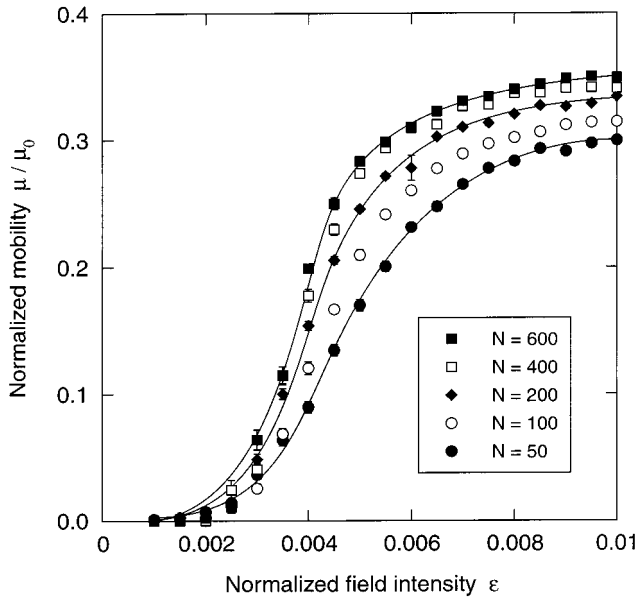

Figure 5. Normalized mobility of a polyelectrolyte in a 3D microchannel as a function of normalized field intensity ϵ, for various molecular sizes N. The plotted values are an average over multiple (10−30) simulations, and error bars represent the standard error on the mean (most are smaller than the size of the points). Solid lines are drawn over the $N = 50$, $N = 200$, and $N = 600$ data to guide the eye.

$\nu = 1$ for an extended chain or $\nu = {}^3/_4$ for a two-dimensional self-avoiding coil.) We therefore write $\Delta F \sim sT - s^{1+\nu}E$, and we find that the critical contour length s_c for the onset of escape satisfies $s_c{}^\nu \sim (T/E)$. Since the span of the inserted coil itself scales as s^ν, we have $x_c \sim s_c{}^\nu$, and we recover eq 2 for x_c. Hence, the linear dependence of x_c on $1/\epsilon$ is a robust feature of the system, in the sense that it does not depend on the conformation of the chain inside the gap. On the other hand, these considerations affect the expression for the mean trapping time, since we now obtain a dependence of the form $\tau_{trap} \sim \exp[(\epsilon_0/\epsilon)^{1/\nu}]$ as opposed to eq 3.

IV. Simulation Results

A. Mobility. The mobility of the polyelectrolytes in the microchannel is plotted as a function of the applied electric field in Figure 5. We find that long molecules are faster than shorter ones for practically all field values. Note that the data for small fields ($\epsilon < 0.003$) are not very reliable, as they bear large uncertainties due to very long trapping times. In the region of best separation (around $\epsilon = 0.004$), we find that the mobility increases by about 30% when the chain length is increased by a factor 4, in good agreement with the experimental observations of Han et al.[1] We also note that the shape of the mobility curves qualitatively reproduces that of the experimental ones very well. The separation capability of the device appears to be retained at high fields, which is also consistent with Han's more recent report,[2] although it may be exaggerated in our simulation for reasons we will discuss later. We should recall that, depending on the type of separation one is trying to achieve, the resolution of the device may actually be limited by the diffusion of the molecules inside the device, so that the best separation on the mobility graph does not necessarily correspond to the best resolution regime for an actual separation device (see section IV.E).

B. Molecular Conformation. It follows from the simple theory of trapping and escape reviewed in section III that the fraction of the monomers directly in contact with the well−gap boundary is an important factor in determining the separation capability of the device. Larger molecules escape faster mostly because they expose more monomers to this boundary (along the y direction), favoring multiple hernia nucleations (see Figure 4b), hence increasing the escape probability and therefore the overall electrophoretic mobility. Furthermore, the electric forces deform the molecule during trapping, pressing it against the vertical wall, thus accentuating the difference between small and large molecules. Of course, such deformation along the gap can play a role only if it takes place faster than the escape time of the chain. To investigate this conformational contribution to the separation process, we plot in Figure 6a−c the Cartesian components of the radius of gyration of the polymer (X_g, Y_g, Z_g, with $R_g{}^2 = X_g{}^2 + Y_g{}^2 + Z_g{}^2$) as a function of the position of the center of mass of the polymer coil inside the channel (mod L), for a field intensity $\epsilon = 0.004$. The graphs are normalized to the values X_{g0}, Y_{g0}, and Z_{g0} obtained for chains in an open channel, i.e., one without constrictions. The radius of gyration of a polymer coil is a highly fluctuating quantity (i.e., $\langle(R_g - \langle R_g\rangle)^2\rangle \sim \langle R^2{}_g\rangle$). Hence, we applied a moving window averaging filter[23] over the raw data to obtain the smooth curves shown in Figure 6; we estimate an uncertainty of 5% for these smoothed curves.

These graphs provide a clear picture of the typical conformations adopted by the molecules as they travel down the channel. At $x = 0$, X_g is large because the molecules have extended while crossing the previous entropic barrier in a slithering motion. This is also clearly observed, for example, in video microscopy movies captured by Han et al.[24] The relative extension of the molecules along the x axis is more important for long chains, although it decreases at some point due to the finite length of the gap. (The two ends of a $N = 600$ molecule can lie in two different wells, and only the middle extended portion of the chain then contributes to the increase in X_g.) At $x = 100$, the molecules leave the narrow gap and undergo rapid compression along x, which can be a consequence of two factors. First, the large gradient of electric field in x at the exit of the gap favors an accumulation of monomers (much like a traffic jam in a region of sudden low velocity). Second, the field lines are diverging in z (see Figure 3) and can thus stretch the chains along that axis, thereby inducing a decrease in X_g. (The plot of Z_g near $x = 100$ shows that

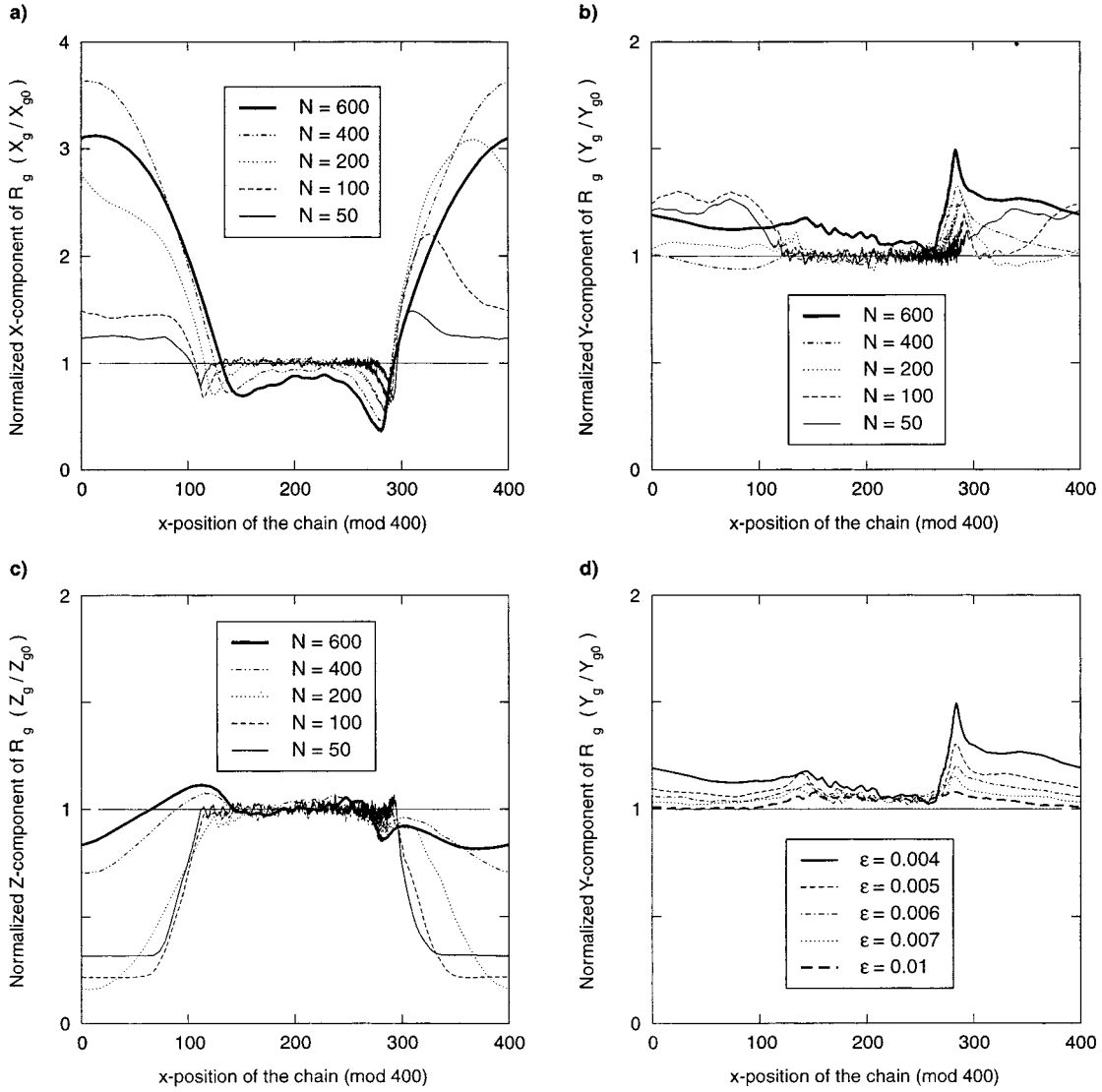

Figure 6. (a), (b), and (c) respectively show the average of the normalized X, Y, and Z component of the radius of gyration R_g as a function of the position (mod $L = 400$) of the center of mass of the polyelectrolyte inside the channel, for a field $\epsilon = 0.004$. The well−gap interface where trapping occurs is located at $x = 300$, and the horizontal line at 1 represents the value for chains in a channel without constrictions. (d) shows another graph for the Y component, but for a single molecular size $N = 600$ and various values of the electric field ϵ. The magnitude of the deformation near the well−gap interface at $x = 300$ is seen to decrease with increasing field strength.

this second process is only significant for the two longest chains.) Further inside the well region, the molecules recover their normal radius of gyration values, except for the $N = 600$ chain which does not have time to relax completely. (For $N = 600$, the top and bottom walls confine the coil slightly and hence may inhibit rotational relaxation modes.)

The actual differentiation of molecular sizes occurs near $x = 300$, as the molecules reach the thin gap through which they must somehow escape. The coils undergo a large compression in the x direction coupled with an important extension along the y direction, as they are pressed against the vertical wall at $x = 300$ (since Z_{g0} is typically larger than the size of the gap). The small dip in the Z_g value at this point for large N indicates that the converging field lines also slightly squeeze large molecules vertically. In Figure 7, we plot the value of Y_g (not normalized) at its peak near the gap entrance as a function of molecular size. For $\epsilon = 0.004$, the size along y scales as $N^{0.75}$ (the scaling law for the size of self-avoiding chain in two dimensions), so the number of monomers available for hernia nucleation also scales as $N^{0.75}$ (since it is just proportional to the length of the coil directly exposed to the gap). The deformation is thus more pronounced for larger molecules. In other words, the molecule adopts the conformation of an "ellipsoidal pancake" near the well−gap interface.

The deformation of the molecule during trapping also depends on the strength of the electric field. One may think that the compression of the molecule against the gap interface (and therefore its extension in y) will increase with field, but this is not so. In fact, we find just the opposite. As the field increases, the probability that any given hernia will actually lead to a complete escape of the molecule also increases, and long molecules simply do not have time to deform before escape is initiated. The situation then resembles Figure 4a. To confirm this, we provide in Figure 6d plots of Y_g for different values of the field strength ϵ. The four curves are similar, but the extension along y near the well−gap interface gradually *fades out* as ϵ rises (and this

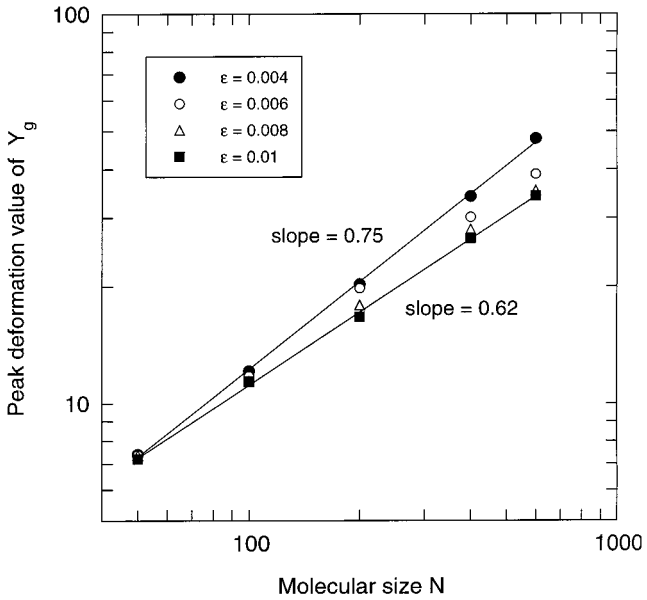

Figure 7. Maximum value of the Y component of the radius of gyration R_g during trapping as a function of molecular size N, for different values of the field ϵ.

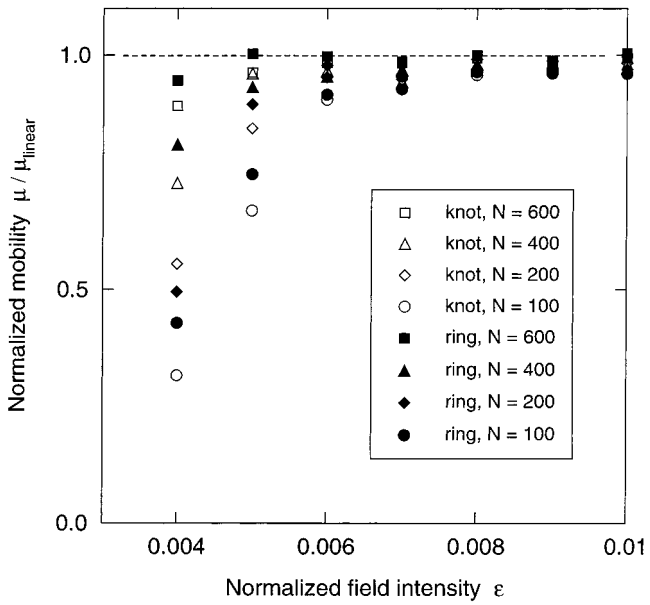

Figure 8. Mobility of ring and trefoil-knotted molecules inside the microfluidic device, normalized to the mobility of a linear chain of the same size. We see an overall downward trend in the mobility as the molecules become more compact. The uncertainties on the plotted values at low field (not shown) are quite large and may account for the crossing of the knot and ring curves for $N = 200$ and $N = 400$.

holds true for the other molecular sizes as well). This effect is also apparent in Figure 7 where the scaling law for the size of the coil gradually returns toward the usual $N^{0.58}$ (for a self-avoiding walk in three-dimensions) as the field increases, indicating that the deformation becomes minimal when the field is very large. On the other hand, we verified that between $\epsilon = 0.001$ and $\epsilon = 0.004$ the field is too weak to induce larger deformations. Hence, there is a tradeoff between the field-driven molecular deformation and the hernia nucleation time: the best separation occurs near $\epsilon = 0.004$, the highest field value for which the average trapping time is at least as long as the deformation time for all molecular sizes N (see section IV.E for more details). This key finding is consistent with the idea that the contact area between the molecule and the well−gap interface plays a determinant role in the separation process. Our results confirm that the size and the deformation of a molecule as a whole control to a large extent its electrophoretic behavior in the microdevice.

C. Topoisomers. As further evidence of the importance of the overall size, shape, and deformation of the molecules in the separation process, we consider topoisomers. By "topoisomer" we mean molecules that have the same number of monomers but different topologies. For example, we can compare the mobility of linear, ring, and trefoil-knotted molecules in the microchannel. Since a change in topology generally implies a change in the overall size R_g of the molecule (rings are smaller than linear chains, and knots are smaller than rings), we expect to see a separation according to topology, the more compact molecules travelling more slowly inside the channel. Indeed, we see in Figure 8 that rings have a smaller mobility than linear chains and that knots, in general, are slower than rings. Moreover, we find that at high fields the topoisomer separation capability vanishes, which is consistent with our assertion that the ratio between the molecular deformation time and the trapping time is a determinant variable in this system.

D. Critical Hernia Nucleation Size. In this section we look at the escape process on a smaller scale, in that we give a measure of the critical insertion length x_c, i.e., the maximum distance a chain can venture inside the gap region without initiating the escape of the whole molecule. We also refer to x_c as the critical hernia nucleation size, since it sets a demarcation between small temporary hernias inside the gap and the ones that continue to grow and eventually lead to the escape of the whole molecule. In fact, this length corresponds to the position of the maximum of the free energy barrier, according to the theory reviewed in section III. The critical length x_c is hardly tractable experimentally but can further validate the theory through the verification of the prediction $x_c \sim 1/E$. Note that the theory also suggests that x_c is independent of the molecular size N, which seems reasonable since hernia nucleation is a local process for long enough chains (for which Z_{g0} is larger than the gap).

To extract the value of x_c from simulations, we periodically record the position of the monomer having the largest x coordinate; we call this monomer the leading monomer, or *leader*, and denote its position by x_{lead}. Small samples of the leading monomer position as a function of time are provided in Figure 9. From these data we determine when the chain is trapped and plot a distribution of the leader's position (mod L) exclusively during trapping. Examples of such distributions are shown in Figure 10. We can describe the tail of the distribution inside the gap (i.e., to the right of the well−gap interface located at $x = 300$) rather well with a number of simple functions, including the exponential $\rho(x_{lead}) = \rho_0 e^{-x_{lead}/x_c}$, where ρ_0 is a normalization factor. We thus extract the value of x_c directly by fitting this function to the data. (We restrict the fit to the middle $^3/_5$ of the points to avoid the slight deviations at the gap entrance and the noisy tail.)

In Figure 11 we show the results of our analysis for all molecular sizes N as a function of $1/\epsilon$. We first observe that for large chains the critical length does exhibit a clear $1/\epsilon$ dependence, as indicated by the

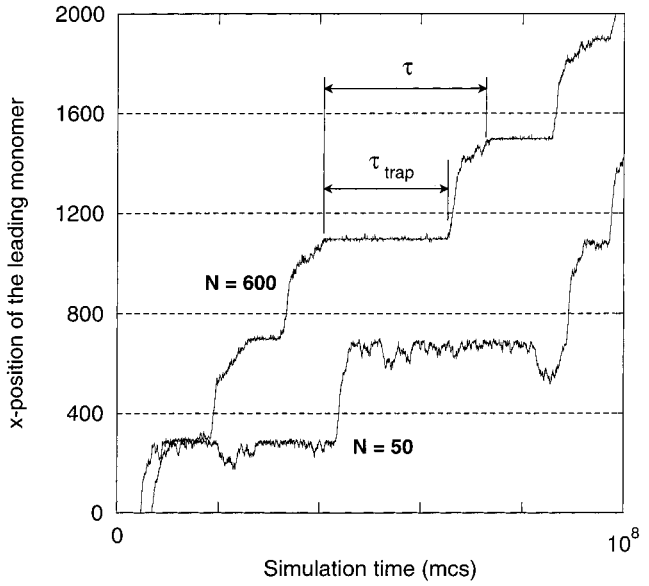

Figure 9. Position of the leading monomer as a function of simulation time (with arbitrary offsets), for two molecular sizes and a field strength of $\epsilon = 0.004$. Labels identify what we define as the trapping time τ_{trap} and the total transit time τ. For the calculation of the critical hernia nucleation size, we only use the data corresponding to trapped configurations. Horizontal dashed lines indicate the periodic boundaries of the channel.

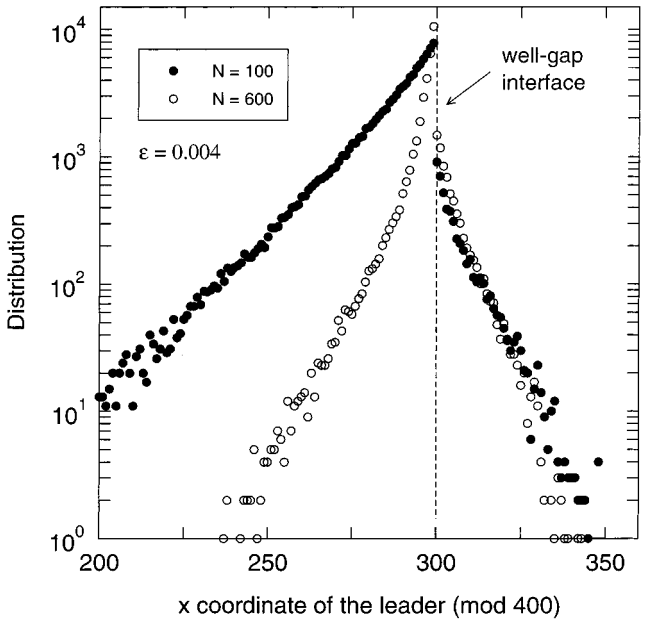

Figure 10. Unnormalized distribution of the position of the leading monomer during trapping events, for two molecular sizes, and $\epsilon = 0.004$. The vertical dashed line indicates the position of the well−gap interface ($x = 300$).

straight line fit over the $N = 600$ data. For the two smallest chains $N = 50$ and $N = 100$, x_c seems to level off at some point, indicating that there is probably a change of regime when there is not enough monomers left in the well to sustain trapping. Another feature apparent in Figure 11 is a slight molecular size dependence, as x_c is slightly larger for the $N = 50$ and $N = 100$ chains. We attribute this size dependence to the fact that small chains more frequently enter the gap head first or tail first, whereas longer chains almost exclusively enter the gap through hernia nucleation. The subtle difference between these two processes is not

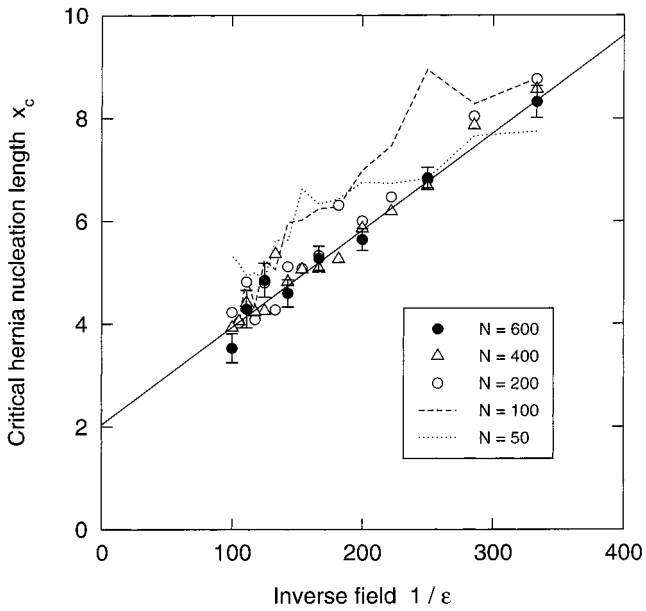

Figure 11. Critical hernia nucleation size x_c as a function of $1/\epsilon$, for five different molecular sizes. Typical error bars, included for the $N = 600$, are calculated using a Monte Carlo regression technique[23] on each point. The solid line is a linear fit for $N = 600$.

captured by the simple free energy model suggested in ref 1, but we verified that for ring molecules, which do not have any dangling ends, this dependence of x_c on N is lost (data not shown). Considering that the ends of a chain have more entropy than other parts of the chain, we do expect the critical length x_c to increase for end insertion because the entropic barrier the polymer has to overcome is then effectively higher.

The position of the leading monomer also provides valuable information about the thermal fluctuations of the center of mass of the molecule during trapping, which are clearly apparent from the distributions at the left of the well−gap interface in Figure 10. On the basis of these distributions, we see that the molecules can backtrack inside the well over an appreciable distance. As a matter of fact, these fluctuations constitute an additional size-separation mechanism favoring higher mobilities for longer chains inside the device. Indeed, smaller molecules carry a smaller total charge and are thus more loosely *bound* to the interface by the electric field. This implies that they can move away from the gap interface and travel backward inside the well after unsuccessfully trying to enter the gap for a while (as seen in Figure 9 for $N = 50$). Consequently, they are more rarely in the vicinity of the well−gap interface, and this contributes to slow them down compared to longer molecules.

E. Trapping Time Statistics. The theory in section III predicts the functional form of the mean trapping time τ_{trap} for the molecules inside the entropic trap array. The trapping time corresponds to the average time the molecules have to wait before their attempts to escape from the trap succeed; it is directly related to the height of the free energy barrier ΔF_{max} for the penetration of the molecule inside the gap region.

For our analysis, we define τ_{trap} as in Figure 9, i.e., as the interval between the first arrival of the leading monomer within $10a$ of the position of the well−gap interface along x and the onset of the escape of the whole molecule, defined as the moment of nucleation of the

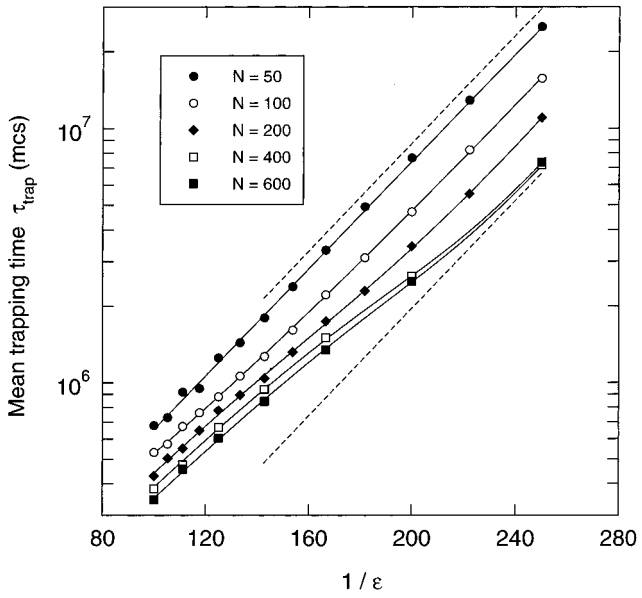

Figure 12. Mean trapping time τ_{trap} as a function of $1/\epsilon$. The dashed lines indicate the slope of the curve for $N = 50$, and solid lines are superimposed on each data set to guide the eye.

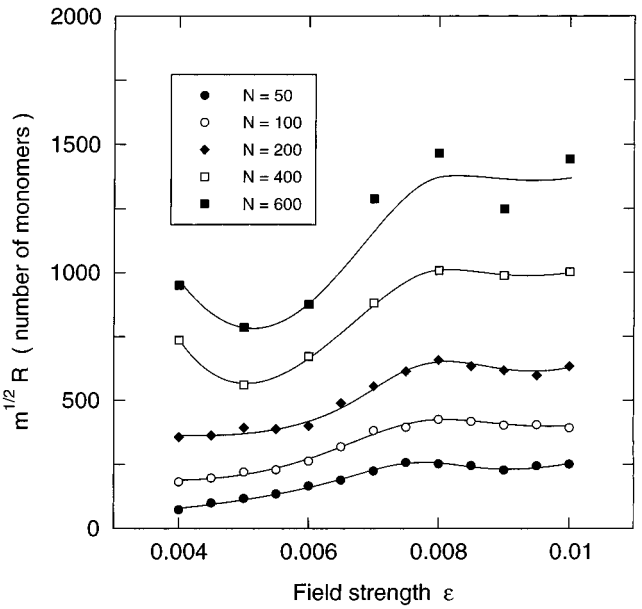

Figure 13. Resolution of the device as a function of the field strength ϵ for different molecular sizes. The values plotted here should be divided by $\sqrt{m}$ to obtain the actual resolution for a channel with m traps. The resolution corresponds to the smallest size difference that can be resolved (measured in number of effective monomers, each of which corresponds to approximately 150 base pairs in the case of dsDNA); the smaller the value, the better the resolution. Solid lines are sketched to guide the eye.

hernia that eventually grows to cross the whole gap region. (We use the threshold $10a$ to compensate for the coarse sampling during the simulation.) In Figure 12 we plot the results for τ_{trap} as a function of $1/\epsilon$, for five different molecular sizes N. We find that for $N = 50$ the data indeed follow the prediction $\tau_{trap} \sim \exp(\epsilon_0/\epsilon)$, as seen from the essentially perfect straight line on the semilog plot. For large molecular sizes, however, the lines exhibit an upward curvature as $1/\epsilon$ decreases, which we explain in terms of our foregoing argument about global molecular deformations. When the field is high, the trapping time becomes very short, so short in fact that molecules do not have time to deform completely before escape is initiated. (The decreased deformation at high fields is shown in Figure 6d.) Hence, long chains tend to behave like shorter ones since only one entrance blob has time to form. The dependence of the mobility on molecular size N thus decreases, and the lines get closer together as at higher fields ϵ in Figure 12.

In fact, the point of departure of the curves from the straigth line in the graph gives a rough estimate of the deformation time τ_d for each molecular size at a given field. We verified that the deformation time estimated in this way is consistent with the approximation $\tau_d(N,\epsilon) \sim R_g/v_{well} \sim R_g/(\mu_0\epsilon) = N^{3/5}/(\mu_0\epsilon)$, where v_{well} is the electrophoretic speed of the molecule inside the well. In other words, the shape and offset of the curves in Figure 12 are controlled by the prefactor τ_0 in eq 3, where τ_0 depends on both the molecular size N and the field strength ϵ. This dependence is different from that derived in ref 22, for example, because of the molecular deformation magnitude and time scale issues. Finally, we also note that in their respective linear portions all the curves in Figure 12 have similar slopes. This is consistent with the Han et al. findings[1] and confirms that ϵ_0 in eq 3 does not depend on the molecular size N. From a fit of the $N = 50$ data we obtain $\epsilon_0 \approx 0.025$.

F. Resolution. From a pratical point of view, and depending on the type of separation one wishes to achieve, the resolution of the separation device might become the limiting factor for reliable detection of the separated species. Thinking in terms of total elution time $t_e(N,\epsilon)$ for the molecules inside the channel (in *finish line mode*, where all molecules travel an equal distance), we can give a measure of the resolution using the ratio of the temporal peak width $w_t(N,\epsilon)$ associated with the population of molecules having a certain molecular size N to the elution time difference between different peaks. Thus, we may express the resolution $R(N,\epsilon)$ as follows:

$$R(N,\epsilon) = \frac{w_t(N,\epsilon)}{\partial t_e/\partial N} \tag{4}$$

Note that according to this definition a decrease in R corresponds to an improvement of the resolution. The value of R also coresponds to the smallest difference in molecular size one can expect to resolve. (Keep in mind, however, that we are here talking about effective monomers which represent, for example, more than 100 base pairs.) It is convenient to rewrite eq 4 in terms of the molecular mean transit time $\tau(N,\epsilon)$ over one period L of the channel, a quantity for which the simulations provide good statistics (given that the molecules visit enough traps, which holds true in our case when $\epsilon \geq 0.004$). Taking $t_e(N,\epsilon) = m\tau(N,\epsilon)$, where m is the number of traps in the device and $\sigma_\tau(N,\epsilon)$ as the standard deviation of τ, and assuming that $w_t = \sigma_\tau\sqrt{m}$ (successive transit times are uncorrelated, so the total variance is the sum of the variance for each trap), we obtain

$$R(N,\epsilon) = \frac{1}{\sqrt{m}}\left(\frac{\sigma_\tau(N,\epsilon)}{\partial\tau(N,\epsilon)/\partial N}\right) \tag{5}$$

In Figure 13 we plot the factor in brackets on the right-hand side of eq 5 as a function of field for different molecular sizes. We find that the optimal resolution

occurs at low field. Only for the two longest chains do we see a shallow minimum near $\epsilon = 0.005$; for the three other chain lengths, we can only say that the optimal resolution lies below $\epsilon = 0.004$. The resolution generally worsens as the field increases but levels off for $\epsilon > 0.008$. Our graph indicates that the value of $\sqrt{m}R$ for molecules with $N = 100$, corresponding roughly to 15 kbp, lies between 165 and 430 bond-fluctuation monomers, i.e., between 25 and 65 kbp. This is consistent with published experimental data[2] from which we can estimate $\sqrt{m}R \approx 50$ kbp for this molecular size in a channel of $m = 3750$ traps. Along those lines, our simulations predict that for molecular sizes of $N = 600$, or nearly 100 kbp, a 1 kbp resolution is achievable with about 15 000 traps.

V. Discussion

The first point we must address is the correspondence between the simulations and the real microchannel device of Han et al.[1,2] As demonstrated throughout the Results section, our simulations reproduce what is found experimentally: an increase in mobility with molecular size, the overall shape of the mobility curves, the simple dependence of the trapping time and the critical hernia nucleation size on the inverse of the field strength, and an optimal resolution near the low field limit of operation. In addition, simulations allowed us to study microscopic details of the molecular conformations, the trapping events, and the escape processes. Such details, not normally accessible experimentally, clarify the fundamental mechanisms behind this first microfluidic separation system based entirely on entropic effects. We have not, however, compared simulation and experimental results on a strictly quantitative basis. Such a correspondence is generally difficult to establish in Monte Carlo work and in our work in particular because of a discrepancy in the values of the electric field strength. Case in point, if we take $q \approx 300e$ (DNA carries two electronic charge per base pair, and one effective monomer represents in very coarse terms 150 base pairs), $a \approx 20$ nm, and $T \approx 300$ K, we find that $\epsilon = 0.005$ corresponds to a global electric field of $E = \Delta V_0/L \approx 20$ V/m, whereas the typical field values in experiments are over 2000 V/m. Three factors can account for this. First, we do not include counterions in our simulations, and thus we do not account for the increased local friction they exert locally on the polyelectrolyte (although the free-draining property of the coil, a consequence of this local friction, is preserved by our Monte Carlo approach). Second, as pointed out in section II.C, the force needed to mechanically pin the polyelectrolyte in the real device is reduced by a factor $\sim N^{2/5}$; hence, the electric force needed to overcome the steric barrier is underestimated by the same factor. Third, the experiments are performed at high ionic strength;[1,2] hence, counterion condensation[25] may come into play, reducing the effective charge of the dsDNA strand. All of these effects suggest that we underestimate the electric field strength in the simulations. Note also that any electroosmotic flow in the device (although reportedly quenched[2]) would reduce the speed of the DNA molecules and demand a stronger field. Despite the offset introduced in our simulations by omitting these effects, our findings remain qualitatively sound.

Our simulation results uphold the idea that the main separation mechanism in the device relies on the size *and* the deformation of the molecule as a whole. Longer molecules move faster through the microchannel simply because they have more opportunities to escape from the entropic traps. We established that the scaling law for the size of the chain along the well−gap interface during trapping is $N^{0.75}$ in the best resolution regime. This lies midway between the assumption of Han et al.[1] for the contact area between the coil and the gap (based on the scaling law for the size of a self-avoiding walk in three dimensions, i.e., $N^{0.58}$) and that of Sebastian's model[22] (in which the number of monomers available for hernia nucleation scales as N^1). We also found that the deformation of the molecule depends on the magnitude of the driving field. When the field is too weak, it cannot deform the coil substantially, and when it is too strong, molecules escape from the trap swiftly and do not have time to deform. Current models fail to take these dynamical phenomena into account, although such effects appear important for the future design and optimization of microdevices that manipulate macromolecules. On the basis of our findings for the mobility of topoisomers, we also predict that the device of Han et al. would be able to fractionate not only rings and simple knots but also a variety of other topological arrangements, such as branched polymers and catenane structures (interlocked rings), provided that they differ in size or in deformability.

As explained at the end of section IV.D, the thermal motion of the center of mass of the molecule inside the well region serves as an additional separation mechanism favoring a higher mobility for longer chains. In fact, this second mechanism is probably the only one remaining at high field, when the contributions of the overall shape and deformation have already vanished (as argued from the topoisomer results above). The magnitude of the molecular-scale thermal motion decreases with increasing field strength. Consider for example a simplified picture in which the whole molecule is represented by a point particle with charge Nq. Taking x_g as the position of the well−gap interface, the probability distribution of the position of this particle for $x < x_g$ would follow a probability density $\sim e^{-N\epsilon(x_g - x)/a}$ (e.g., the left side of the distribution in Figure 10). The magnitude of the thermal fluctuations is then embodied in the factor $1/N\epsilon$, so for a 100-fold increase in ϵ the extent of the fluctuations is reduced 100-fold. Hence, in light of the fact that the real field strength is about 2 orders of magnitude larger than the simulation field strength, this second separation mechanism is probably irrelevant for the current experimental conditions. At such high fields the molecules remain in contact with the well−gap interface practically all the time during trapping, even in what corresponds to our "low-field" regime. Fluorescence video microscopy sequences captured by Han et al.,[24] in which individual dsDNA molecules are never seen moving against the field inside the wells, support this claim.

From the simulation data we extracted the mean trapping time τ_{trap} and the critical hernia nucleation size x_c, two quantities expected to depend in a simple way on $1/\epsilon$ according to a simple free energy model. We find good agreement with this prediction for both τ_{trap} (provided we understand the deviations caused by long deformation time scales) and x_c (given that we acknowledge the limit imposed by a finite chain length). According to our comment at the end of section III, the linear dependence of $\log(\tau_{trap})$ on $1/\epsilon$ identified in Figure 12 suggests that the hernias are indeed well extended

along the field direction inside the gap for $\epsilon \geq 0.004$.

Last, we found that the resolution of the device is generally optimal at low field and that after deteriorating over midrange field strengths, it levels off around $\epsilon = 0.008$. This is interesting at first sight because it suggests that high-field—thus high-speed—separation may be possible without loss of resolution in this microdevice. But we recall that the good resolution calculated at high field stems from the separation caused by the global thermal motion of the center of mass of the molecule, an effect most likely absent in experiments. The plateau in R at high fields may therefore only occur in the simulation context. On the other hand, the trend observed at low field agrees with the general experimental observation that as the field decreases, the improved separation of molecular sizes wins out over the increased dispersion due to longer trapping time,[2] leading to better resolution.

We are currently using our Monte Carlo simulations to explore new regimes of operations and optimize the geometry of this entropic separation device using the information we have gathered on the dominant physical mechanisms at play.

Acknowledgment. We acknowledge the support of the Natural Science and Engineering Research Council of Canada for a Research Grant to GWS and scholarships to F.T. and the University of Ottawa for scholarships to F.T. In addition, we acknowledge J. Han, S. W.Turner, and H. G. Craighead for useful discussions about their microdevice experiments.

References and Notes

(1) Han, J.; Turner, S. W.; Craighead, H. G. *Phys. Rev. Lett.* **1999**, *83*, 1688.
(2) Han, J.; Craighead, H. G. *Science* **2000**, *288*, 1026.
(3) Volkmuth, T. D. W. D.; Wu, M. C.; Austin, R. H.; Szabo, A. *Phys. Rev. Lett.* **1994**, *72*, 2117.
(4) Chou, C.-F.; Austin, R. H.; Bakajin, O.; Tegenfeldt, J. O.; Castelino, J. A.; Chan, S. S.; Cox, E. C.; Craighead, H.; Darnton, N.; Duke, T.; et al. *Electrophoresis* **2000**, *21*, 81.
(5) Turner, S. W.; Perez, A. M.; Lopez, A.; Craighead, H. G. *J. Vac. Sci. Technol. B* **1998**, *16*, 3835.
(6) Ertaş, D. *Phys. Rev. Lett.* **1998**, *80*, 1548.
(7) Duke, T. A. J.; Austin, R. H. *Phys. Rev. Lett.* **1998**, *80*, 1552.
(8) Derényi, I.; Astumian, R. D. *Phys. Rev. E* **1998**, *58*, 7781.
(9) Chou, C.-F.; Bakajin, O.; Turner, S. W. P.; Duke, T. A. J.; Chan, S. S.; Cox, E. C.; Craighead, H. G.; Austin, R. H. *Proc. Natl. Acad. Sci. U.S.A.* **1999**, *96*, 13762.
(10) Hammond, R. W.; Bader, J. S.; Henck, S. A.; Deem, M. W.; McDermott, G. A.; Bustillo, J. M.; Rothberg, J. M. *Electrophoresis* **2000**, *21*, 74.
(11) van Oudenaarden, A.; Boxer, S. G. *Science* **1999**, *285*, 1046.
(12) Griess, G. A.; Rogers, E.; Serwer, P. *Electrophoresis* **2001**, *22*, 981.
(13) Chou, H.-P.; Spence, C.; Scherer, A.; Quake, S. *Proc. Natl. Acad. Sci. U.S.A.* **1999**, 11.
(14) Slater, G. W.; Guo, H. L.; Nixon, G. I. *Phys. Rev. Lett.* **1997**, *78*, 1170.
(15) Carmesin, I.; Kremer, K. *Macromolecules* **1988**, *21*, 2819.
(16) Deutsch, H. P.; Binder, K. *J. Chem. Phys.* **1991**, *94*, 2294.
(17) Allen, M. P.; Tildesley, D. J. *Computer Simulations of Liquids*; Oxford University Press: New York, 1990.
(18) Long, D.; Viovy, J.-L.; Ajdari, A. *Biopolymers* **1996**, *39*, 755.
(19) Long, D.; Viovy, J.-L.; Ajdari, A. *Phys. Rev. Lett.* **1996**, *76*, 3858.
(20) Long, D.; Ajdari, A. *Electrophoresis* **1996**, *17*, 1161.
(21) Long, D.; Dobrynin, A. V.; Rubenstein, M.; Ajdari, A. *J. Chem. Phys.* **1998**, *108*, 1234.
(22) Sebastian, K. L.; Paul, A. K. R. *Phys. Rev. E* **2000**, *62*, 927.
(23) Press, W. H.; et al. *Numerical Recipes in C*; Cambridge University Press: New York, 1992; p 650.
(24) http://www.hgc.cornell.edu/biofab/entropic.htm, 1999.
(25) Manning, G. S. *Q. Rev. Biophys.* **1978**, *11*, 179.

MA0110406